

Two-Dimensional Nonlinear Wave Dynamics in Blasius Boundary Layer Flow Using Combined Compact Difference Methods

JC Chen* and Weijia Chen

Abstract—Turbulence transition in Blasius boundary layer flows arises from nonlinear wave generation, interaction, and amplification in the flow. The nonlinear wave dynamics depend on the intricate phase synchronization of the propagating waves. Numerical simulation of the process encounters challenges in the forms of achieving sufficient computational resolution, dealing with truncated computational domains, and control of numerical errors. Application of high-order, optimized Combined Compact Difference numerical methods help to mitigate these issues and achieve realizations of nonlinear wave dynamics during turbulence transition. Validations of the numerical results versus linear stability theory and another numerical study, as well as, a grid independence study attest to the accuracy and robustness of the model.

Index Terms—turbulence, transition, combined compact difference, nonlinear wave dynamics, grid independence

I. INTRODUCTION

The classical work Schubauer and Skramstad, 1947 [1] conducts a famous experiment to examine the topic of boundary layer turbulence transition. The experiment entails a vibrating ribbon that is placed at the base of the inlet to a flow channel and acts to introduce perturbations into the flow. The perturbations convert to disturbance waves that travel downstream. As the disturbance waves propagate downstream, they will begin to interact with one another in progressive stages of transition towards flow turbulence. Initially, the wave interactions are linear in the linear instability stage [2]. Further downstream, the wave interactions will evolve to become nonlinear. The nonlinear interactions will spawn a secondary instability in the flow. The secondary instability will eventually become unsustainable and break down into turbulence. The stages of transition up to the linear instability stage are well-understood presently. The linear wave interactions can be described accurately with the Orr-Sommerfeld (OS) equation of linear stability theory. Chen and Chen, 2010 [3] offers an excellent study of the linear stage of turbulence transition. However, once the waves undergo nonlinear interactions, the transition phenomenon becomes mysterious

and is the subject of much current research.

A subsequent classical work, Klebanoff, *et al.*, 1962 [4] would shed illuminating insight into the nonlinear stage of transition. As transition to turbulence can occur via multiple pathways, Klebanoff, *et al.*, 1962 [4] studies the pathway that has come to bear the namesake of its author, K-type transition. When the amplitude of the initial perturbation exceeds 1% of the mean flow, the K-type transition mechanism activates to induce an explosive amplification of waves leading to breakdown into turbulence. Klebanoff, *et al.*, 1962 [4] observes definitive and reproducible behavior of nonlinear wave interactions beginning with the formation of the first set of waves from the perturbation known as the fundamental waves. The fundamental wave exercises a fecundity that begets second and third harmonics of successively higher wave frequencies. The harmonics would then cluster in wave packets as they traverse downstream. Within the packets, the waves interact and synchronize. The phase synchronization of the waves results in explosive spikes in the observed wave oscillations. These observations have become bespoke signature features of nonlinear turbulence transition [4].

Additional classical works would ensue. Kachanov and Levchenko, 1984 [5] and Kachanov, 1994 [6] reveal another possible pathway towards turbulence called the N-type transition. The N-type transition facilitates a more controlled pathway to turbulence, evoked by a lower amplitude of the initial disturbance than K-type transition. As such, the N-type transition transpires with measurably exponential amplification of waves as contrasted with the incontinent explosion in the K-type. Also, the N-type transition generates harmonics of lower frequencies than the K-type. For more details, Herbert, 1988 [7] offers an excellent review of the physical processes occurring in the nonlinear transition stage.

The perspicacity of the aforementioned procession of classical works, though worthy of fete, has only begun to enervate the confounding complexity of the turbulence transition phenomenon. The nature of turbulence transition remains shrouded in mystery to the present time.

II. ISSUES OF CONCERN

The numerical simulation of boundary layer turbulence transition meets with several challenges. The simulation endeavor must successfully contend with these issues of concern so that it can attain accurate and precise realizations of the transition process.

Manuscript received 5 May, 2011; supported by Ministry of Education Grant RG 4/07.

*JC Chen, Corresponding Author, Nanyang Technological University, School of Civil and Environmental Engineering, Singapore (phone: +65 6790-5273; fax: +65 6790-5273; e-mail: jimchen@ntu.edu.sg)

Weijia Chen, Nanyang Technological University, School of Civil and Environmental Engineering, Singapore (e-mail: ch0003ia@e.ntu.edu.sg)

A. Computational Resolution

The wave interaction dynamics underlying the transition to turbulence presents a view of the process from the perspective of periodic oscillations of the disturbance velocities in wave form. A concomitant perspective views the process in terms of the formation and deformation of physical flow structures during transition. Some of the commonly observed flow structures include the Λ -vortex, Ω -vortex, high shear layer, and turbulent streaks [3]. An important physical flow structure of note is the formation of turbulent eddies strewn intermittently throughout the flow. The intermittent turbulent eddies also experience progeneration where first generation eddies beget second and third generations in cascading fashion ([8], [9], and [10]). The posterior eddies will sequentially decrease in length and time scales, imposing taxing demands on the computational power required to visualize them. Chen, 2009 [8] offers an excellent exposition on the eugenics of turbulent eddy progeneration. The numerical simulation must have the computational capacity to reach the necessary level of computational resolution.

Further exacerbating the situation is the concept of three-dimensionality. During the transition towards turbulence, the generated waves will acquire a three-dimensional characteristic. The formation of three-dimensional waves represents a key development in the transition towards turbulence. Saric, *et al.*, 2003 [11] explains that the three-dimensional waves arise from crossflow and centrifugal instabilities occurring in flow regions with pressure gradients. The three-dimensional nature of the flow is the critical element that leads to rapid generation of additional harmonics and their subsequent explosive or exponential amplification. Orszag and Patera, 1983 [12] notes that, during wave interactions, the two-dimensional waves are unstable to the presence of even infinitesimal three-dimensional waves and will amplify exponentially from the encounter. Orszag and Patera, 1983 [12] systematically illustrates that the combination of vortex stretching and tilting terms in the governing Vorticity Transport Equation accelerates the growth of waves. Both vortex stretching and tilting are required to produce the accelerated growth of waves [12]. Both are three-dimensional phenomena and thus, concurringly underline the important role of three-dimensionality in turbulence transition. Reed and Saric, 1989 [13] and Herbert, 1988 [7] offer excellent reviews of the mechanisms that cause the formation of three-dimensional waves. Numerical visualization of three-dimensional waves incurs arduous computational demands.

Even further immiseration in regard to computational demands comes in the form of the critical Reynolds number. The putative work, Orszag and Kells, 1980 [14], explains that, for the transition to turbulence to be sustainable, the flow Reynolds number must exceed a critical threshold value. The fact that a critical Reynolds number exists for turbulence transition has been corroborated by other works of Orszag and Patera, 1983 [12] and Saric, *et al.*, 2003, [11]. Towards the study of nonlinear wave interaction dynamics, the critical Reynolds number carries a vexatious implication. The resolution of computational grids needed to realize turbulent flow structures scales exponentially with the Reynolds number (number of grid points $\sim Re^{9/4}$) [3].

Hence, for transition to occur, the Reynolds number must surpass a critical threshold, and the numerical visualization of the transition process at that Reynolds number requires a computational grid that scales exponentially with it. The exponential correlation between the Reynolds number and grid causes the computational demands to quickly reach impractical levels for even typical turbulent flows.

Clearly then, due to the amalgamation of these issues, microscopic length scales of turbulent eddies, three-dimensionality, and critical Reynolds number, the computational demands weigh onerously on numerical simulations of turbulence transition [15]. Computational capacity of the present time cannot meet such demands for flows of physically realistic dimensions within practical simulation runtime limits. The limitation in computational capacity leads to a follow-up challenge, well-renowned as the Open Boundary Condition (OBC) problem.

B. Open Boundary Condition Problem

Because present-day computational capacity cannot practically realize turbulence transition for flows of realistic physical dimensions, the computational domain must be truncated to maintain satiable computational demands. This truncation creates its own problems. Questions now arise regarding what should be the correct boundary conditions stipulated at the points of truncation. In general, for boundary layer flows, the domain will be truncated at the freestream and outflow boundaries. For the freestream boundary, because it lies transverse to the prevailing flow, the disturbance vorticity will decay rapidly along that direction, making the boundary conditions there relatively manageable. However, the case of the outflow boundary stands as a formidable challenge, because it lies in-line with the flow direction and the downstream direction of the amplifying waves. The propagating waves will exit the domain at the outflow boundary while potentially still containing appreciable wave amplitudes. How to correctly define the outflow boundary conditions endures as a topic of much longstanding controversy and debate. The outflow boundary conditions must be defined in such a way as to prevent the exiting waves from reflecting back into the domain to cause numerical errors. This issue is known as the Open Boundary Condition (OBC) problem.

Sani and Gresho, 1994 [16] provides an interesting review of OBC's based on dialogue from two mini-symposia, Mini-symposium on Outflow Boundary Conditions for Incompressible Flow, that took place within the 6th and 7th International Conference on Numerical Methods in Laminar and Turbulent Flow, 1989 and 1990, respectively [16]. The mini-symposia posed four problems and invited contributions on defining the OBC's for them. The four problems were the backward-facing step, stratified backward-facing step, vortex shedding past a cylinder, and Poiseuille-Bernard channel flow [16]. Many different forms of the OBC were tested. Sani and Gresho, 1994 [16] reports on the effectiveness of these boundary conditions when applied to the four problems. Ultimately, the correct choice of OBC also varies with the specific flow conditions of each problem. So, the correct stipulation of the OBC remains inconclusive and elusive. Other studies that propose their solutions for non-reflecting OBC's include Jin and Braza,

1993 [17], Hedstrom, 1979 [18], Rudy and Strikwerda, 1980 [19], and Christer and Johansson, 1993 [20]. Another excellent review of OBC's is given in Gresho, 1991 [21].

Since the correct definition of the OBC proves to be querulous, perhaps then, it would be expedient to eschew the topic by appealing to the convenience of using a buffer domain. A buffer domain implements a damping function near the outflow that would dissipate the waves prior to their exit. Other works that practice this strategy include Street and Macaraeg, 1989 [22] and Meitz and Fasel, 2000 [23].

The insertion of an artificial buffer domain onto an artificial truncation of that domain merely trades one problem for another. Unsurprisingly, a new problem emerges, this time in the form of grid-mesh oscillations. The buffer domain inserts a discontinuity into the domain that will generate oscillating numerical errors of high wave numbers that can flow back upstream to distort the true wave dynamics. Furthermore, the buffer domain forcibly damps waves that potentially could still be amplifying. The coerced damping against the amplifying will of the waves results in violent oscillations with clearly visible shaking of the wave motion, as the waves struggle against the suppression of the buffer domain [15]. Grid-mesh oscillations declare a very important issue of contention in the simulations of turbulence: control of numerical errors.

C. Numerical Errors

Nonlinear wave generation, interaction, and amplification in boundary layer turbulence transition rely heavily on the intricate minutiae underlying synchronization of the phases and amplitudes of the propagating wave packets. As such, the presence of pernicious numerical errors exacts a noisome toll on the accuracy and precision of the numerical visualizations with potentially disastrous consequences. One of the sources of numerical errors emanates from the buffer domain. The buffer domain prevents the exiting waves from reflecting back upstream but at the cost of introducing its own errors in the form of grid-mesh oscillations. Other types of errors can be introduced from the numerical discretization of the governing equations of the flow. With finite difference discretizations, numerical dissipation, dispersion, and aliasing errors become relevant.

Dissipation errors pertain to the accurate depiction of the amplitudes of the propagating waves. The flow contains natural viscous dissipative forces. So, dissipation errors can emerge simply from inaccurate accounting for the effects of viscous dissipation ([2], [24], and [25]). In addition, the numerical discretization can generate pseudo-dissipative mechanisms in the simulation that otherwise should not be present at all ([2], [24], and [25]). These would be numerical dissipation errors. Dissipation errors impact the amplification behavior within the wave interaction dynamics, and wave amplification is a key component of the turbulence transition process.

Dispersion errors deal with the phase velocities of the traveling waves, as well as, the relative velocities amongst waves within a group or packet. The effects of dispersion errors cause the wave velocities to drift away from their true speeds ([2], [24], and [25]). This can lead to incorrect lagging or acceleration of the traveling waves, or even worse, a false total reversal in the direction of propagation.

Dispersion errors affect the phase synchronization of the interacting waves, and this synchronization is the flywheel that drives wave generation, interaction, and amplification in boundary layer turbulence transition [15].

Perhaps, the most dyspeptic prospects egress from aliasing errors. The interactions of the propagating waves produce additional waves with increasing wave numbers. For simulations with insufficient numerical resolution, the high wave number waves would need to be interpolated or aliased onto the grid as lower wave number waves. The incorrect representation of the high wave number wave as a lower wave number wave will cause numerical instabilities that culminate in the apprehensive scenario of numerical blow-up ([26] and [27]). Indeed, aliasing error threatens potential disaster if the numerical simulation does not adequately address its catastrophic influence.

So then, the discussion heretofore should elucidate the detracting and devastating aspects of numerical errors. Therefore, the abeyance of numerical errors poses a mandate of utmost importance. Combined compact difference numerical methods offer a viable tool for surmounting the preceding jeremiad in regards to the challenges confronting numerical simulations of wave dynamics occurring in Blasius boundary layer flow [15]. Chen and Chen, 2011 [15] offers an excellent discussion of this topic.

III. PROBLEM DEFINITION

A. Governing Equations

The governing equations for turbulence transition in Blasius boundary layer flow are the Navier-Stokes (NS) equations. For better ease of defining the flow conditions at the boundaries, the NS equations undergo a conversion to its variant form, the Vorticity Transport Equation (VTE). Chen and Chen, 2010 [3] provides copious discussions on the transformation procedure and its mathematical implications. The total set of governing equations for two-dimensional flows comprise the VTE given in (1), the Velocity-Poisson's Equation in (2), and the continuity condition in (3):

$$\frac{\partial \omega}{\partial t} + u \frac{\partial \omega}{\partial x} + v \frac{\partial \omega}{\partial y} = \frac{1}{Re} \frac{\partial^2 \omega}{\partial x^2} + \frac{\partial^2 \omega}{\partial y^2}, \quad (1)$$

$$\frac{1}{Re} \frac{\partial^2 v}{\partial x^2} + \frac{\partial^2 v}{\partial y^2} = -\frac{\partial \omega}{\partial x}, \text{ and} \quad (2)$$

$$\frac{\partial^2 u}{\partial x^2} = -\frac{\partial^2 v}{\partial x \partial y}. \quad (3)$$

where u is the velocity in the x -direction, v is the velocity in the y -direction, and ω is the vorticity. The numerical model can be extended to three-dimensional flows once the accuracy of the two-dimensional model has been established. The flow parameters u , v , and ω consist of the steady, time-independent base flow components, u_B , v_B , and ω_B , and time-dependent components, u' , v' , and ω' , that account for the disturbance:

$$u(x, y, t) = u_B(x, y) + u'(x, y, t), \quad (4)$$

$$v(x, y, t) = v_B(x, y) + v'(x, y, t), \text{ and} \quad (5)$$

$$\omega(x, y, t) = \omega_B(x, y) + \omega'(x, y, t). \quad (6)$$

Figure 1 shows the flow domain. Truncations to the domain occur at the freestream boundary CD and outflow

boundary BC. The perturbation is introduced into the flow at the location of the black block in the form of a blowing and suction strip.

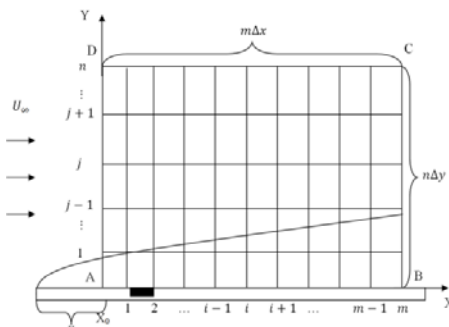


Fig. 1. The computational flow domain.

B. Boundary Conditions for the Steady Flow Field

The base flow is solved from the steady-state form of (1) that does not include the term $\frac{\partial \omega}{\partial t}$ ([28] and [29]). Proceeding are the boundary conditions for the base flow.

Inflow Boundary Conditions

A feasible method for defining the inflow boundary condition explicitly specifies the flow variables from approximate solutions of the NS equations, for example, by solving the Blasius equation. This study prescribes the inflow boundary conditions at AD of Fig. 1 for the flow parameters u_B , v_B , and ω_B , as well as, their first and second derivatives from the Blasius equation solution.

Wall Boundary Conditions

The boundary conditions at the wall are:

$$u_B = 0, \quad (7)$$

$$v_B = 0, \text{ and} \quad (8)$$

$$\frac{\partial v_B}{\partial y} = 0. \quad (9)$$

The wall vorticity is calculated from:

$$\frac{\partial \omega_B}{\partial x} = -\frac{\partial^2 v_B}{\partial y^2}. \quad (10)$$

Equations (7) and (8) implement the no-slip and non-penetration boundary conditions, respectively. Equation (9) stems from the continuity equation. Equation (10) derives from (2), which is similar to the derivation of Fasel, 1976 [28]. The VTE requires specification of the continuity condition at the boundary to ensure that the velocity field is divergence-free. The issue of defining the boundary conditions so as to preserve a divergence-free flow field provokes much continuing debate in the field. Incorporating (7) and (8) to the derivation of (9) satisfies this condition. Fasel, 1980 [30] and Daube, 1992 [31] provide detailed discussions of the wall boundary conditions.

Freestream Boundary Conditions

The boundary conditions at the freestream are:

$$u_B = 1, \quad (11)$$

$$\frac{\partial v_B}{\partial y} = 0, \quad (12)$$

$$\omega_B = 0, \quad \frac{\partial \omega_B}{\partial y} = 0, \text{ and} \quad \frac{\partial^2 \omega_B}{\partial y^2} = 0. \quad (13a-c)$$

Equation (12) derives from the continuity equation to again ensure a divergence-free velocity field. The freestream boundary occurs approximately three boundary layer thicknesses above the wall. The boundary condition then assumes the flow to be irrotational, and so, the vorticity vanishes [28].

Outflow Boundary Conditions

The outflow boundary conditions prescribe the second derivatives of the parameters u , v , and ω to be zero [28]:

$$\frac{\partial^2 u_B}{\partial x^2} = 0, \quad (14)$$

$$\frac{\partial^2 v_B}{\partial x^2} = 0, \text{ and} \quad (15)$$

$$\frac{\partial^2 \omega_B}{\partial x^2} = 0. \quad (16)$$

C. Boundary Conditions for the Unsteady Flow Field

Inflow Boundary Conditions

The inflow boundary condition for the unsteady flow field assumes no disturbances there. So, the values of u' , v' and ω' , as well as, their first and second derivatives become zero at the inflow boundary.

Wall Boundary Conditions

The wall boundary conditions of the unsteady flow field remain the same as for the steady flow with the exception of the disturbance-generating strip (black block in Fig. 1). Based on Meitz and Fasel, 2000 [23], and Bhaganagar, *et al.*, 2002 [29], and Fasel and Konzelmann, 1990 [32], the disturbance generation uses a function $d(x,t)$ to compute v' in a region between x_1 and x_2 of the computational domain. The boundary conditions in this region are:

$$v' = d(x,t), \quad (17)$$

$$\frac{\partial \omega'}{\partial x} = -\frac{\partial^2 v'}{\partial y^2} - \frac{1}{Re} \frac{\partial^2 d}{\partial x^2}, \text{ and} \quad (18)$$

$$d(x,t) = \mu f(x) \sin(\beta t). \quad (19)$$

with μ used to adjust the amplitude and β as the disturbance frequency. The function $f(x)$ is:

$$f(x) = \begin{cases} 24.96\xi^6 - 56.16\xi^5 + 31.2\xi^4 \\ -24.96\xi^6 + 56.16\xi^5 - 31.2\xi^4 \end{cases} \quad (20)$$

$$\xi = \frac{x - x_1}{x_{st} - x_1} \quad x_1 < x < x_{st} \quad (21)$$

$$\xi = \frac{x_2 - x}{x_2 - x_{st}} \quad x_{st} < x < x_2. \quad (22)$$

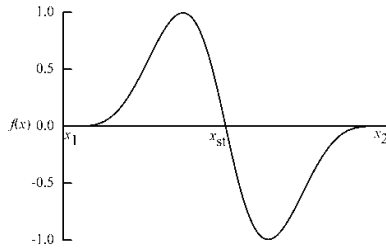
Figure 2 shows the function $f(x)$. It satisfies the conditions:

i. The disturbances start and end with zero amplitude $f(x_1) = f(x_2) = 0$

ii. Continuity for first derivative at the beginning and the end of the strip:

$$\frac{df}{dx}(x_1) = \frac{df}{dx}(x_2) = 0$$

iii. Conservation of total mass: $\int_{x_1}^{x_2} f(x) dx = 0$.


 Fig. 2. Function $f(x)$ over the blowing and suction strip.

Freestream Boundary Conditions

The freestream boundary conditions are:

$$\frac{\partial v'}{\partial y} = -\frac{\alpha}{\sqrt{\text{Re}}} v', \quad (23)$$

$$\omega' = 0, \quad \frac{\partial \omega'}{\partial y} = 0, \quad \text{and} \quad \frac{\partial^2 \omega'}{\partial y^2} = 0. \quad (24 \text{ a-c})$$

Based on linear stability theory, these conditions assume that the disturbance velocities decay exponentially as a function of the linear wave number α towards the freestream boundary. Meitz and Fasel, 2000 [23] and Bhaganagar, *et al.*, 2002 [29] implement similar freestream boundary conditions.

Outflow Boundary Conditions

The OBC problem at the outflow boundary receives aid from a buffer domain. The buffer domain damps ω between a designated point $x = x_B$ and the outflow boundary by multiplying ω to a damping function $T(L_b)$, shown in Fig. 3:

$$T(L_b) = \frac{0.9778 + 1.3074 \cos(\pi L_b) + 0.33187 \cos(2\pi L_b) + 0.0022278 \cos(3\pi L_b)}{1 + 0.63707 \cos(\pi L_b) + 0.17261 \cos(2\pi L_b)} \quad (25)$$

$$L_b = \frac{x_B - x}{x_B - x_M}. \quad (26)$$

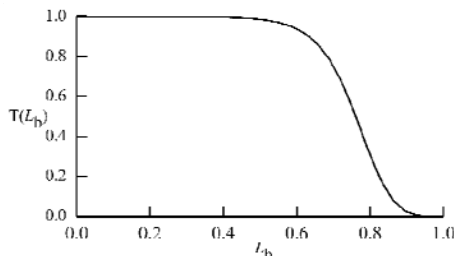


Fig. 3. The damping function.

After damping, the outflow boundary conditions become:

$$\frac{\partial^2 u}{\partial x^2} = \frac{\partial^2 v}{\partial x^2} = \frac{\partial^2 \omega}{\partial x^2} = 0. \quad (27)$$

The insertion of the buffer domain interjects a discontinuity that produces grid-mesh oscillating errors with high wave numbers in the order of the grid spacing. To preserve the accuracy and precision of the numerical simulation, the grid-mesh oscillations must be suppressed along with other types of numerical errors, dissipation, dispersion, and aliasing errors.

IV. NUMERICAL METHOD

A. Combined Compact Difference Schemes

With lower dissipation and dispersion errors than conventional finite difference methods while using the same stencil width, high-order combined compact difference (CCD) schemes provide the dual-advantages of accuracy of

simulations and control of numerical errors. The CCD scheme combines the discretization for the function, f , its first derivative, f'_i , and second derivative, f''_i , with a , b , and c as the coefficients of the numerical scheme and h as the grid size:

$$h \sum_{i=-2}^2 a_{1,i} f'_i + h^2 \sum_{i=-2}^2 b_{1,i} f''_i + \sum_{i=-2}^2 c_{1,i} f_i = 0 \quad \text{and} \quad (28)$$

$$h \sum_{i=-2}^2 a_{2,i} f'_i + h^2 \sum_{i=-2}^2 b_{2,i} f''_i + \sum_{i=-2}^2 c_{2,i} f_i = 0. \quad (29)$$

A 5-point CCD scheme involves points at $i = -2, -1, 0, 1, 2$. To derive a CCD scheme of 12th-order accuracy, there will be 15 coefficients each for (28) and (29). The parameters $b_{p,2}$ ($p = 1, 2$) should be set as 1 for normalization. Then, $b_{p,0}$ and $b_{p,1}$ are free for selection. The other 12 parameters are obtained from matching the Taylor series up to 12th-order as:

$$a_{p,-2} = \frac{17}{54} b_{p,0} + \frac{11}{8} b_{p,1} + \frac{65}{2}, \quad (30a)$$

$$a_{p,-1} = -\frac{80}{27} b_{p,0} - 7b_{p,1} - 128, \quad (30b)$$

$$a_{p,0} = -3b_{p,0} - \frac{27}{2} b_{p,1} - 216, \quad (30c)$$

$$a_{p,1} = \frac{8}{27} b_{p,0} - 5b_{p,1} - 64, \quad (30d)$$

$$a_{p,2} = \frac{1}{216} b_{p,0} + \frac{1}{16} b_{p,1} - \frac{19}{2}, \quad (30e)$$

$$b_{p,-1} = -\frac{8}{9} b_{p,0} - 3b_{p,1} - 64, \quad (30f)$$

$$b_{p,-2} = \frac{1}{36} b_{p,0} + \frac{1}{8} b_{p,1} + 3, \quad (30g)$$

$$c_{p,-2} = \frac{869}{864} b_{p,0} + \frac{821}{192} b_{p,1} + \frac{399}{4}, \quad (30h)$$

$$c_{p,-1} = -\frac{76}{9} b_{p,0} - 22b_{p,1} - \frac{1312}{3}, \quad (30i)$$

$$c_{p,0} = \frac{17}{2} b_{p,0} + \frac{27}{4} b_{p,1} + 216, \quad (30j)$$

$$c_{p,1} = -\frac{28}{27} b_{p,0} + \frac{34}{3} b_{p,1} + 96, \quad \text{and} \quad (30k)$$

$$c_{p,2} = -\frac{7}{288} b_{p,0} - \frac{23}{64} b_{p,1} + \frac{307}{12}. \quad (30l)$$

The discretizations of the spatial derivative terms

involving $\frac{\partial^2}{\partial x^2}$, $\frac{\partial}{\partial y}$, and $\frac{\partial^2}{\partial y^2}$ in (1) to (3) use 12th-Order

Centered-Difference Combined Compact Difference schemes hereafter referred to as CCCD12. The high order of the numerical discretizations here will suppress dissipation and dispersion errors. The derivation of the coefficients for the Centered-Difference discretizations for $\frac{\partial^2}{\partial x^2}$, $\frac{\partial}{\partial y}$, and $\frac{\partial^2}{\partial y^2}$ prescribes $b_{1,0} = -10152/35$, $b_{1,1} = 1696/35$, $b_{2,0} = 0$, and $b_{2,1} = -32$.

The discretization of the term $u \frac{\partial \omega}{\partial x}$ uses a 12th-Order Upwind-type Combined Compact Difference scheme hereafter referred to as UCCD12. The upwind nature of this

discretization scheme will suppress the grid-mesh oscillations arising from the buffer domain.

B. Temporal Scheme

The discretization of the temporal derivative in (1) uses a 4th-order 5-6 alternating stages Runge-Kutta (RK) scheme based on Hu, *et al.*, 1996 [33]. Here, the vorticity transport equation (1) can be written as:

$$\frac{\partial \omega}{\partial t} = F(\omega) \tag{31}$$

where the operator F contains the discretization of spatial derivatives. An explicit, *s*-stage low storage RK method advances the solution from time level *t* to *t* + Δ*t* by:

$$K_i = \Delta t F(\omega^t + r_i K_{i-1}) \tag{32}$$

with *i* = 1, ..., *s* and *r_i* as the RK coefficients. Then, the temporal discretization proceeds by:

$$\omega^{t+\Delta t} = \omega^t + K_s. \tag{33}$$

Hu, *et al.*, 1996 proposes a 5-6 alternating stages RK method [33], which means that from time level *t* to *t* + Δ*t*, there are 5 stages; then, from *t* + Δ*t* to *t* + 2Δ*t*, there are 6 stages. Different RK coefficients *r_i* of the respective 5- and 6-stage schemes are used and coupled for optimization. The method of Hu, *et al.*, 1996 only considers the temporal discretization errors [33]. On the other hand, the current study optimizes the coefficients *r_i* of the temporal RK scheme together with the coefficients of the upwind type UCCD12 scheme for the spatial *x*-derivative $\frac{\partial \omega}{\partial x}$ using the one-dimensional wave equation.

C. Optimization of Numerical Method

Optimization of the coefficients for the discretizations for $u \frac{\partial \omega}{\partial x}$ and the 4th-order 5-6 RK temporal scheme seeks the objective of minimizing their numerical errors. The methodology of the optimization applies these discretizations to the one-dimensional wave equation:

$$\frac{\partial \omega}{\partial t} + u \frac{\partial \omega}{\partial x} = 0 \tag{34}$$

with periodic boundary conditions in the *x*-direction. The procedure optimizes the coefficients of discretization for (34). The logic of the optimization correlates the attributes of the numerical errors of (34) to how the discretization methods may perform for the VTE.

Equation (34) can be simplified as:

$$\frac{\partial \omega}{\partial t} = F(\omega) \tag{35}$$

where the operator F contains the discretization of the spatial derivative. To analyze the errors of the numerical method, the amplification factor \bar{A} of the schemes can be considered, which is the ratio between the numerical solution at time levels *t* + Δ*t* and *t* in spectral space. If the general RK scheme in (32) and (33) is applied, it can be shown that the spatial Fourier transform of (35) can lead to:

$$\hat{\omega}^{t+\Delta t} = \hat{\omega}^t \left(1 + \sum_{i=1}^s \hat{r}_i \Delta t \hat{F} \right) \tag{36}$$

where $\hat{\omega}^t$ and \hat{F} are the spatial Fourier transforms of ω and the spatial operator F, respectively [34]. The \hat{r}_i 's are

the constants related to the coefficients in (32) with the following relationship:

$$\hat{r}_2 = r_s, \tag{37a}$$

$$\hat{r}_3 = r_s r_{s-1}, \tag{37b}$$

$$\vdots \tag{37c}$$

$$\hat{r}_s = r_s r_{s-1} \cdots r_2.$$

The amplification factor, a measure of the degree to which $\hat{\omega}^t$ will grow with successive progressions in *t*, becomes:

$$\bar{A} = \frac{\hat{\omega}^{t+\Delta t}}{\hat{\omega}^t} = \left(1 + \sum_{i=1}^s \hat{r}_i \Delta t \hat{F}(w_1) \right). \tag{38}$$

In this study, the first four parameters are fixed as $\tilde{r}_1 = 1$, $\tilde{r}_2 = 1/2!$, $\tilde{r}_3 = 1/3!$, and $\tilde{r}_4 = 1/4!$ to match the Taylor series; so, the RK scheme is 4th-order [33]. The remaining parameters are optimized to control the dispersion and dissipation errors in different Fourier wave number spectrums. The Fourier transformation of the spatial operator \hat{F} for (38) is:

$$\hat{F} = -l \frac{U}{\Delta x} w_1 \tag{39}$$

where $l = \sqrt{-1}$ and w_1 can be obtained from the modified wave number analysis to be discussed in Section IV D. Let the amplification factors of the first and the second time steps be \bar{A}_5 and \bar{A}_6 . Substituting (39) into (38) for each time step gives:

$$\bar{A}_5 = \left(1 + \sum_{i=1}^5 \hat{r}_{5,i} (-iCFL w_1) \right) \text{ and} \tag{40a}$$

$$\bar{A}_6 = \left(1 + \sum_{i=1}^6 \hat{r}_{6,i} (-iCFL w_1) \right) \tag{40b}$$

where:

$$CFL = \frac{u \Delta t}{\Delta x} \tag{41}$$

is the Courant-Friedrichs-Levy (CFL) number. Then, the amplification factor for these two steps combined is equal to $\bar{A}_5 \bar{A}_6$. Similar to the traditional expression of modified wave number analysis for spatial errors, the real and imaginary parts of w_1^G represent the global dispersion and dissipation errors at each temporal step, respectively:

$$(w_1^G)_R = -\frac{\text{angle}(\bar{A}_5 \bar{A}_6)}{2CFL} \text{ and} \tag{42a}$$

$$(w_1^G)_I = \frac{1}{2} \ln |\bar{A}_5 \bar{A}_6|. \tag{42b}$$

Suppose the time of the physical wave propagation in the computation domain is *t*. During this period of time *t*, the relative position between the phases of the numerical solution and the exact solution is:

$$\text{relative phase position} = \frac{(w_1^G)_R}{w}. \tag{43}$$

The total damping from the numerical dissipation becomes: relative wave amplitude = $\exp[(w_1^G)_I t]$. $\tag{44}$

Under a certain CFL number, w_1^G is a function of 7 free parameters, $b_{1,0}$, $b_{1,1}$, $b_{2,0}$, $b_{2,1}$, $\hat{r}_{5,5}$, $\hat{r}_{6,5}$, and $\hat{r}_{6,6}$. These parameters can be adjusted to assign the following attributes to the global scheme:

(a) To ensure accurate discretization schemes, w_1^G should agree with the corresponding scaled wave number w in a desirable range. The range selected for optimization is from $w = 0$ to 2.0.

(b) To generate strong dissipation to suppress grid-mesh oscillations, the imaginary part of w_1^G should have a large negative value from $w = 2.9$ to π .

The scheme is designed according to the above two requirements by minimizing a target function ε :

$$\varepsilon = \int_0^2 \left\{ \sigma \left| (w_1^G)_R - w \right| + (1 - \sigma) \left| (w_1^G)_I \right| \right\} dw + \int_{2.9}^{\pi} \left| (w_1^G)_I \right| + 2.5 \left| dw \right|. \quad (45)$$

where σ is the weight between dispersion and dissipation errors. The scheme should satisfy the stability constraint:

$$(w_1^G)_I \leq 0 \quad (46)$$

so that the amplification factor $\bar{A}_5 \bar{A}_6 \leq 1$. The free coefficients that are locally-optimized to minimize ε are obtained by the MATLAB function 'fmincon'. The optimization strongly depends on the particular choice of the parameter σ in (45) and is also sensitive to the initial guess. Since the dissipation errors have an exponential effect on the wave amplitude according to (44), more weight is put on the dissipation error, so that $\sigma = 0.4$. The CFL number is chosen as 0.5. The optimized parameters are:

$$b_{1,0} = -9.839998875523017e+003, \quad (47a)$$

$$b_{1,1} = 7.699986096688637e+002, \quad (47b)$$

$$b_{2,0} = -5.599685487846300e+002, \quad (47c)$$

$$b_{2,1} = -3.198909014492459e+001, \quad (47d)$$

$$\dot{r}_{5,5} = 3.701369047580123e-003, \quad (47e)$$

$$\dot{r}_{6,5} = 1.145504041153636e-002, \text{ and} \quad (47f)$$

$$\dot{r}_{6,6} = 1.634736321150070e-003. \quad (47g)$$

D. Control of Numerical Errors

The effectiveness of the CCCD12 and UCCD12 schemes in controlling numerical errors can be examined using Modified Wave Number analysis. This method takes the Fourier transform of (28) and (29) to consider the numerical errors in spectral space:

$$Iw_1 \hat{f} \sum_{i=-2}^2 a_{1,j} \exp(Iiw) + w_2^2 \hat{f} \sum_{i=-2}^2 b_{1,j} \exp(Iiw) \quad (48)$$

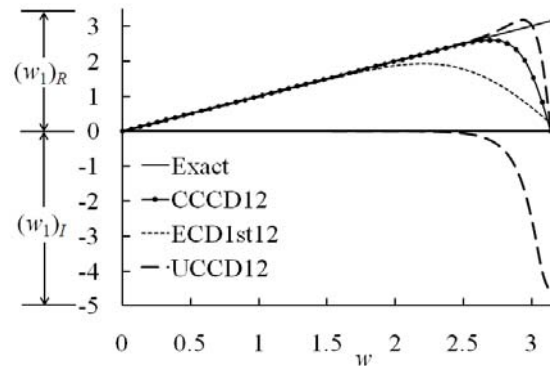
$$+ \hat{f} \sum_{i=-2}^2 c_{1,j} \exp(Iiw) = 0 \text{ and}$$

$$Iw_1 \hat{f} \sum_{i=-2}^2 a_{2,j} \exp(Iiw) + w_2^2 \hat{f} \sum_{i=-2}^2 b_{2,j} \exp(Iiw) \quad (49)$$

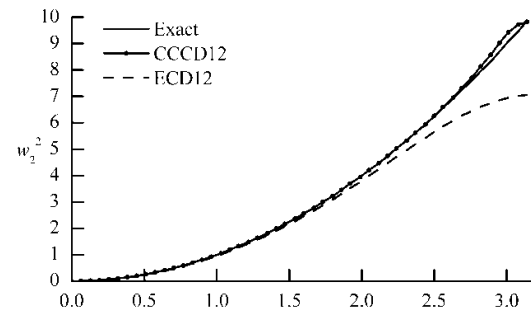
$$+ \hat{f} \sum_{i=-2}^2 c_{2,j} \exp(Iiw) = 0$$

where \hat{f} is the Fourier transform of f , $I = \sqrt{-1}$, and $w = k\Delta x$ is the scaled wave number, the wave number multiplied by the grid size Δx . Due to numerical errors, the scaled wave numbers will be modified. The parameters w_1 and w_2 are the modified scaled wave numbers for the discretizations of the first and second derivatives, respectively. The modified scale wave numbers are complex numbers, whereas the true scale wave numbers are purely real numbers. Figure 4a shows a comparison between the modified and true scaled wave numbers for the first derivative discretizations using the CCCD12, UCCD12, and ECD1st12 (12th-Order Explicit Centered-Difference) schemes. The subscripts R and I represent the real and imaginary parts, respectively.

Deviations of the real part of the modified scale wave number from the true value w will cause dispersion errors. Deviations of the imaginary part, which should be zero since w is a real number, will give rise to dissipation errors. Figure 4a indicates that, the real parts of the modified scale wave number, $(w_1)_R$, for the CCCD12 and UCCD12 schemes remain close to the true value w for a longer range than the ECD1st12 scheme. So, the two foremost schemes should display greater accuracy and lower dispersion errors than the last. The UCCD12 scheme is the only method that exhibits an imaginary part, increasing rapidly at high scaled wave numbers to signify powerful dissipation; this is advantageous for controlling grid-mesh oscillations with high wave numbers. Figure 4b shows a comparison between the modified and true scaled wave number for the second derivative discretizations using the CCCD12 and ECD1st12 schemes. The modified scaled wave number w_2^2 for the CCCD12 scheme clearly remains close to the true value for a longer range than does the ECD1st12.



(a)



(b)

Fig. 4. Comparison between the modified and true scaled wave numbers for (a) the first derivative discretization and (b) second derivative.

The numerical method can be optimized to leverage upon the high accuracies of CCCD12 and UCCD12 schemes and the dissipative tendencies of the UCCD12 scheme at high wave numbers. The idea here is to choose the grid size Δx and coefficients of the UCCD12 and 5-6 RK schemes such that the physical waves for simulation will fall in the range where $(w_1)_R$ remains close to w for accurate realizations. Then, the grid-mesh oscillating errors with high wave numbers will be made to enter into the high dissipation range and be dissipated by the imaginary part $(w_1)_I$.

V. RESULTS AND DISCUSSIONS

Validation against Linear Stability Theory

To establish confidence in the accuracy of the numerical model, its simulations of linear instability can be validated versus the OS equation. Figure 5 shows a comparison between model predictions and the OS equation for (a) the wave propagation trajectory through the neutral stability curve starting from the first branch where the waves begin to amplify and on through the second branch (b) the downstream amplification of the flow parameters u , v , and ω and (c) the wall-normal profiles of the same. The amplitudes are normalized by their respective minimum values, and their logarithms are taken so that the normalized curves have relative minima of 0. The imaginary part of the wave number α_I obtained from the solution of OS equation is used to calculate the theoretical amplification curve [32]:

$$\ln(A/A_{\min}) = -\int_{x_0}^x \alpha_I(x) dx. \quad (50)$$

The amplification behaviors of the flow parameters u , v , and ω in Fig. 5b agree qualitatively well with the solution of the OS equation. The results in Fig. 5c of the transverse profiles of the flow parameters indicate that the simulation results and the OS equation completely overlap, averring excellent agreement.

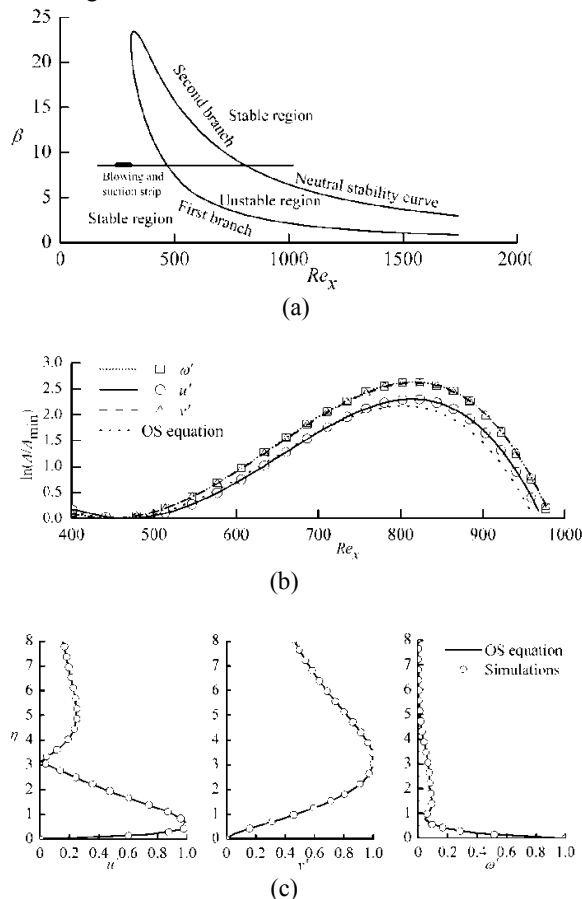


Fig. 5. Validation of the numerical model versus linear stability theory and the OS equation for (a) wave propagation trajectory through the neutral stability curve (b) the downstream amplification of the flow parameters u , v , and ω (c) the wall-normal profiles of the same. Initial disturbance $A_0 = 0.009\%$ of the freestream velocity to maintain linear waves. Downstream x -location $Re_x = \sqrt{x}Re = 400$.

With confidence assured, the matter at hand shifts to the investigation of nonlinear wave generation, interaction, and

amplification in boundary layer turbulence transition. Figure 6 delivers a numerical realization to this effect. The numerical visualization of the downstream evolution of the u -disturbance velocity vividly describes the sequence where disturbance waves manifest then amplify in their amplitudes as they traverse downstream. Indeed, the targeted nonlinear wave dynamics have been realized.

Notice a critical development occurring at the buffer domain. When the waves arrive at the buffer domain, their amplification persists. However, the damping function of the buffer domain forcibly compels the amplifying waves to damp. The struggle between the natural amplifying tendencies of the waves and the forced damping of the buffer domain produces a visible shaking of the waves in the simulation [15]. Numerical errors caused by the disruption from the buffer domain are quite obvious, as is the importance of controlling these errors. The oscillations at the buffer domain tend to have high wave numbers, and the numerical method can eliminate them using the dissipative mechanisms of the UCCD12 scheme shown in Fig. 4 [15].

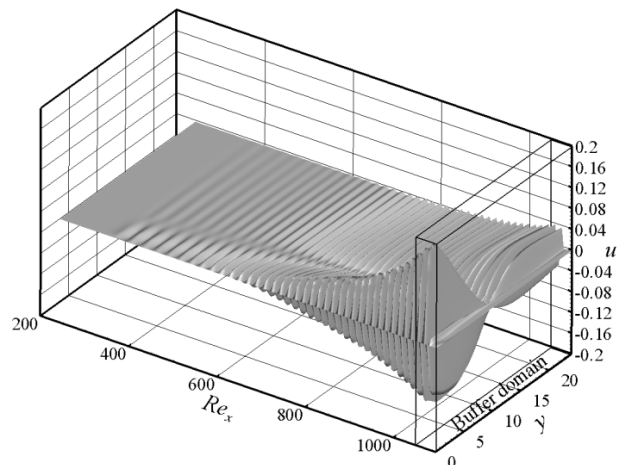


Fig. 6. Downstream amplification behavior of the u -disturbance velocity. Amplitude of initial disturbance $A_0 = 0.3\%$ of the freestream velocity.

Figure 7 shows Fourier decomposition of the flow field in Fig. 6 and depicts four constituent wave components 1F to 4F. The 4F wave has four times the frequency as the 1F. Notice here that the 3F and 4F waves display amplitudes orders of magnitude lower than the 1F and 2F. The microscopic amplitudes of the 3F and 4F waves render them especially vulnerable to distortions from numerical dissipation, dispersion, and aliasing errors. The high-order CCD12 schemes applied to the spatial derivatives control the numerical errors and preserve the low-amplitude waves. Notice further that the 4F wave has a scaled wave number of 2.25, which according to Fig. 4, places it safely in the region before the large dissipative effects at high wave numbers. So, the delicate 4F wave can be protected from this risk.

An important condition for legitimate comparison of the simulation results with those of other studies mandate the solution to be grid independent [25]. Figure 8 provides such an assurance with a grid independence study of the wave decomposition of Fig. 7 using coarse and fine grids. Since the grid spacing Δx is different on the two grids, the waves have different scaled wave numbers w . According to Figs. 4 a and b, these four waves on the coarse grid lie in the effective scaled wave number spectrum from $w = 0$ to 2.5 with small

dispersion errors. For the 1F to 3F waves of the coarse grid in the spectrum $w = 0$ to 1.75, 99% of the wave amplitudes can be preserved. The fine grid solutions of these three harmonics confirm the same amplitude values.

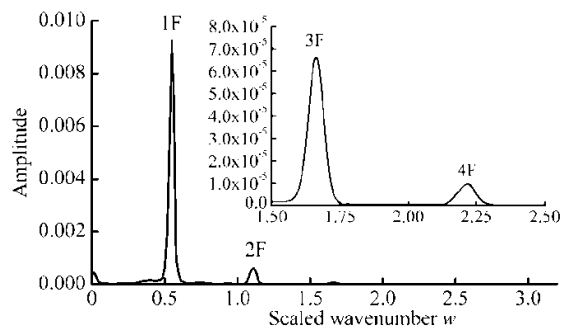


Fig. 7. Fourier transformation of the fully developed flow field given in Fig. 6 at the wall-normal location $y = 0.7$.

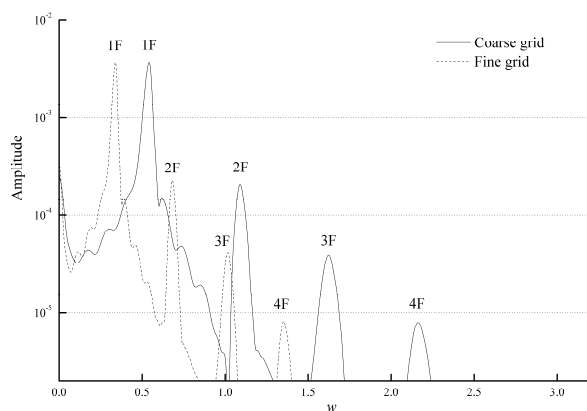


Fig. 8. Grid independence study of the wave decomposition in Fig. 6.

An immediate riposte that inveighs upon this result should be addressed, and that is, the dissipative mechanism of the UCCD12 scheme can destroy high wave number physical waves that may be crucial to the wave interaction dynamics. In fact, the dominance of microscopic-scale eddies in turbulence suggests that high wave number physical waves would seem especially relevant to the process. The remedy to this conundrum would call for rigorous further study of the wave interaction dynamics to astutely demarcate the cut-off point for realizing high wave number waves. Beyond the cut-off point, the waves can be allowed to be dissipated. In Fig. 7, the justification for realizing up to the 4F wave contends that inclusion of higher wave number waves would not produce appreciable changes to the overall disturbance amplification [15].

Figure 9 exhibits qualitative agreement between the model predictions and the numerical study of Bertolotti, *et al.*, 1992 [35] for the amplification behaviors of the 1F and 2F waves. Also, the 1F wave amplifies faster than the prediction from the OS equation due to nonlinear interaction effects. These results attest to the accuracy of the model. Furthermore, the wave behavior can be tuned by adjusting the initial disturbance amplitude and hence, affirms the presence of nonlinear wave interactions.

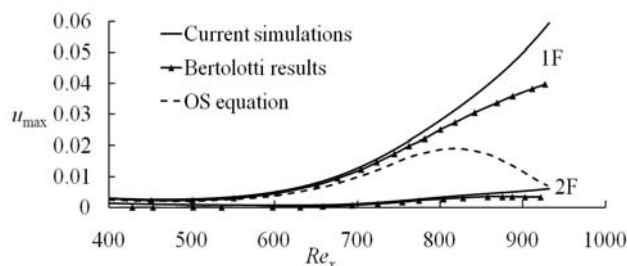


Fig. 9. Comparisons of simulation results of nonlinear amplification of the maximum disturbance velocity u_{\max} with linear stability theory and Bertolotti, *et al.*, 1992 [35].

VI. CONCLUSION

This has been an illuminating discourse on two-dimensional nonlinear wave generation, interaction, and amplification in Blasius boundary layer turbulence flow. This fascinating problem burgeons from the classical works of Schubauer and Skramstad, 1947 [1], Klebanoff, *et al.*, 1962 [4], and Kachanov and Levchenko, 1984 [5]. Important challenges confront the numerical simulation of turbulence transition in terms of considerations for computational resolution, the OBC problem, and control of numerical errors. The numerical model uses high-order, optimized CCD schemes to preserve the physical waves, while dissipating numerical errors with high wave numbers. Numerical realizations resplendently demonstrate the two-dimensional wave dynamics and its underlying constituent components. Validation of the model versus linear stability theory and other works of nonlinear wave dynamics asserts confidence and legitimacy. The numerical model can be extended to three-dimensions to realize the full turbulence transition process and to address the issue of meeting the requisite computational demands.

ACKNOWLEDGMENT

This work is supported by the Ministry of Education Grant RG4/07.

REFERENCES

- [1] G. Schubauer and H. K. Skramstad, "Laminar boundary layer oscillations and stability of laminar flow," *J. Aeronaut. Sci.*, vol. 14, no. 2, pp. 69-78, 1947.
- [2] J. Chen and W. Chen, "Turbulence transition in two-dimensional boundary layer flow: Linear instability," in *Proc. 6th Intl. Conf. Flow Dyn.*, Sendai, Japan, 2009, pp. 148-149.
- [3] J. Chen and W. Chen, "The complex nature of turbulence transition in boundary layer flow over a flat surface," *Intl. J. Emerg. Multidiscip. Fluid Sci.*, vol. 2, no. 2-3, pp. 183-203, 2010.
- [4] P. S. Klebanoff, K. D. Tidstrom and L. M. Sargent, "The three-dimensional nature of boundary-layer instability," *J. Fluid Mech.*, vol. 12, no. 1, pp. 1-34 1962.
- [5] Y. S. Kachanov and V. Y. Levchenko, "The resonant interaction of disturbances at laminar-turbulent transition in a boundary layer," *J. Fluid Mech.*, vol. 138, pp. 209-247, 1984.
- [6] Y. S. Kachanov, "Physical mechanisms of laminar-boundary-layer transition," *Annu. Rev. Fluid Mech.*, vol. 26, pp. 411-482 1994.
- [7] T. Herbert, "Secondary instability of boundary layers," *Annu. Rev. Fluid Mech.*, vol. 20, pp. 487-526, 1988.
- [8] J. Chen, "The law of multi-scale turbulence," *Intl. J. Emerg. Multidiscip. Fluid Sci.*, vol. 1, no. 3, pp. 165-179, 2009.
- [9] G. K. Batchelor, *The theory of homogeneous turbulence. Student's edition*. London: Cambridge University Press, 1953.
- [10] A. S. Monin and A. M. Yaglom, *Statistical fluid mechanics: Mechanics of turbulence II*. Mineola: Dover Publications, 1975.
- [11] W. S. Saric, H. L. Reed and E. B. White, "Stability and transition of three-dimensional boundary layers," *Annu. Rev. Fluid Mech.*, vol. 35, pp. 413-440, 2003.

- [12] S. A. Orszag and A. T. Patera, "Secondary instability of wall-bounded shear flows," *J. Fluid Mech.*, vol. 128, pp. 347-385, 1983.
- [13] H. L. Reed and W. S. Saric, "Stability of three-dimensional boundary layers," *Annu. Rev. Fluid Mech.*, vol. 21, pp. 235-284, 1989.
- [14] S. A. Orszag and L. C. Kells, "Transition to turbulence in plane Poiseuille and plane Couette flow," *J. Fluid Mech.*, vol. 96, no. 1, pp. 159-205, 1980.
- [15] J. Chen and W. Chen, "Numerical realization of nonlinear wave dynamics in turbulence transition using Combined Compact Difference methods," in Lecture Notes in Engineering and Computer Science: Proceedings of The International MultiConference of Engineers and Computer Scientists 2011, IMEC 2011, Hong Kong, 16-18 March, 2011, pp. 1517-1522.
- [16] R. L. Sani and P. M. Gresho, "Resume and remarks on the open boundary condition minisymposium," *Intl. J. Numer. Methods Fluids*, vol. 18, no. 10, pp. 983-1008, 1994.
- [17] G. Jin and M. Braza, "A non-reflecting outlet boundary condition for incompressible unsteady Navier-Stokes calculations," *J. Comput. Phys.*, vol. 107, no. 2, pp. 239-253, 1993.
- [18] G. W. Hedstrom, "Nonreflecting boundary conditions for nonlinear hyperbolic systems," *J. Comput. Phys.*, vol. 30, no. 2, pp. 222-237, 1979.
- [19] D. H. Rudy and J. C. Strikwerda, "A nonreflecting outflow boundary condition for subsonic Navier-Stokes calculations," *J. Comput. Phys.*, vol. 36, no. 1, pp. 55-70, 1980.
- [20] B. Christer and V. Johansson, "Boundary conditions for open boundaries for the incompressible Navier-Stokes equation," *J. Comput. Phys.*, vol. 105, no. 2, pp. 233-251, 1993.
- [21] P. M. Gresho, "Incompressible fluid dynamics: Some fundamental formulation issues," *Annu. Rev. Fluid Mech.*, vol. 23, pp. 413-453, 1991.
- [22] C. L. Streett and M. G. Macaraeg, "Spectral multi-domain for large-scale fluid dynamic simulations," *Appl. Numer. Math.*, vol. 6, no. 1-2, pp. 123-139, 1989.
- [23] H. L. Meitz and H. F. Fasel, "A compact-difference scheme for the Navier-Stokes equations in vorticity-velocity formulation," *J. Comput. Phys.*, vol. 157, no. 1, pp. 371-403, 2000.
- [24] J. Chen and W. Chen, "Combined compact difference method for simulation of nonlinear wave generation, interaction, and amplification in boundary layer turbulence transition," in *Proc. 7th Intl. Conf. Flow Dyn.*, Sendai, Japan, 2010, pp. 82-83.
- [25] W. Chen and J. Chen, "Combined Compact Difference Method for Solving the Incompressible Navier-Stokes Equations," *Intl. J. Numer. Methods Fluids*, in press.
- [26] P. Moin and K. Mahesh, "Direct numerical simulation: A tool in turbulence research," *Annu. Rev. Fluid Mech.*, vol. 30, pp. 539-578, 1998.
- [27] S. L. Lyons and T. J. Hanratty, "Large-scale computer simulation of fully developed turbulent channel flow with heat transfer," *Intl. J. Numer. Methods Fluids*, vol. 13, no. 8, pp. 999-1028, 1991.
- [28] H. Fasel, "Investigation of the Stability of Boundary Layers by a Finite-difference Model of the Navier-Stokes Equations," *J. Fluid Mech.*, vol. 78, no. 2, pp. 355-383, 1976.
- [29] K. Bhaganagar, D. Rempfer and J. Lumley, "Direct Numerical Simulation of Spatial Transition to Turbulence Using Fourth-Order Vertical Velocity Second-Order Vertical Vorticity Formulation," *J. Comput. Phys.*, vol. 18, no. 1, pp. 200-228, 2002.
- [30] Fasel H, "Recent developments in the numerical solution of the Navier-Stokes equations and hydrodynamic stability problems", in W. Kollmann (Ed.), *Computational Fluid Dynamics*, Washington D.C., Hemisphere Publishing Corporation, 1980, pp. 167-279.
- [31] O. Daube, "Resolution of the 2D Navier-Stokes Equations in Velocity-Vorticity Form by Means of an Influence Matrix Technique," *J. Comput. Phys.*, vol. 103, no. 2, pp. 402-414, 1992.
- [32] H. Fasel and U. Konzelmann, "Non-parallel Stability of a Flat-plate Boundary Layer Using the Complete Navier-Stokes Equations," *J. Fluid Mech.*, vol. 221, pp. 311-347, 1990.
- [33] F. Q. Hu, M. Y. Hussaini and J. L. Manthey, "Low-dissipation and low-dispersion Runge-Kutta schemes for computational acoustics," *J. Comput. Phys.*, vol. 124, no. 1, pp. 177-191, 1996.
- [34] C. Hirsch, *Numerical computation of internal and external flows: fundamentals of computational fluid dynamics*. Amsterdam; London: Butterworth-Heinemann, 2007.
- [35] F. P. Bertolotti, T. Herbert and P. R. Spalart, "Linear and nonlinear stability of the Blasius boundary-layer," *J. Fluid Mech.*, vol. 242, pp. 441-474, 1992.